The influence of multiple conformations and paths on rate constants and product branching ratios. Thermal decomposition of 1-propanol radicals

*David Ferro-Costas,** [a,b] *Emilio Martínez-Núñez,* [c] *Jesús Rodríguez-Otero,* [a,c] *Enrique Cabaleiro-Lago,* [c] *Carlos M. Estévez,* [c] *Berta Fernández,* [c] *Antonio Fernández-Ramos** [a,c] *and Saulo A. Vázquez** [c]

[a] Centro Singular de Investigación en Química Biolóxica y Materiais Moleculares (CIQUS), Universidade de Santiago de Compostela, Santiago de Compostela, Spain

[b] LAQV@REQUIMTE, Departamento de Química e Bioquímica, Faculdade de Ciências, Universidade do Porto, 4169-007 Porto, Portugal

[c] Departamento de Química Física, Universidade de Santiago de Compostela, Santiago de Compostela, Spain

ABSTRACT

The potential energy surface involved in the thermal decomposition of 1-propanol radicals was investigated in detail using automated codes (tsscds2018 and Q2DTor). From the predicted elementary reactions, a relevant reaction network was constructed to study the decomposition at temperatures in the range 1000 – 2000 K. Specifically, this relevant network comprises 18 conformational reaction channels (CRCs), which in general exhibit a large wealth of conformers of reactants and transition states. Rate constants for all the CRCs were calculated using two approaches within the formulation of variational transition state theory (VTST). The simplest, one-well (1W) approach considers only the most stable conformer of the reactant and that of the transition state. In the second, more accurate approach, contributions from all the reactant and transition state conformers are taken into account using the multipath (MP) formulation of VTST. In addition, kinetic Monte Carlo (KMC) simulations were performed to compute product branching ratios. The results show significant differences between the values of the rate constants calculated with the two VTST approaches. In addition, the KMC simulations carried out with the two sets of rate constants indicate that, depending on the radical considered as reactant, the 1W and the MP approaches may display different qualitative pictures of the whole decomposition process.

INTRODUCTION

Over the last decades, the investigation of the combustion reactions of oxygenated fuels has attracted much interest due to their potential use as alternatives to conventional petroleum-based fuels. Ethanol is one of the most abundant and commonly used biofuels, and can be employed either as a pure fuel or blended with gasoline.[1-3] In the latter case, the formation of polyaromatic hydrocarbon molecules and soot upon combustion is reduced with respect to that of conventional gasoline,[4] but emission of toxic aldehydes may increase considerably.[5-6] These features are also shared by the smallest alcohol, methanol, as well as by higher alcohols.

The next alcohol, propanol, can be produced from biomass and used as a biofuel.[7-9] Compared to ethanol, the combustion of propanol exhibits a wider plethora of elementary reactions, which depends somewhat on the isomeric form employed, that is, 1-propanol or 2-propanol.[10-18] To investigate the combustion of propanol, and combustion mechanisms in general, it is important to use kinetic models and perform computer simulations as a complement to experimental determinations, due to the tremendous complexity of these chemical processes.[14, 19] For example, the simulations of propanol combustion performed by Frassoldati et al.[13] employed a kinetic model comprising more than 7000 reactions and 300 chemical species. Clearly, simulations of this kind necessarily involve many approximations.

Among the different classes of approximations employed in combustion simulations, we will pay attention to the simplification commonly adopted in systems where the potential energy surface (PES) exhibits multiple conformers and paths, as in the decomposition of 1-propanol. Usually, the energetic profile of the reaction network is simplified by considering only the

lowest-energy rotamers (i.e., conformers obtained by rotations around single bonds). In recent years, the role of multiple conformers and paths has been addressed in the context of variational transition state theory (VTST).[20-22] These studies have led to new improvements and extensions in VTST, known as multistructural and multipath VTST.[22] Multistructural VTST (MS-VTST)[22-27] uses a multifaceted dividing surface and includes the contributions from the different structures (in general, rotamers) of the reactant and the transition state (TS) in the calculation of the rate constant.[23-24] This approach takes into account only the single lowest-energy path associated with the multiple reactant conformers and TS conformers. In multipath VTST (MP-VTST)[22-23, 28-32] a total rate constant is calculated using the contributions from the individual reaction paths that connect reactant conformers with the corresponding TS conformers. Quantum tunneling and variational effects are evaluated for each individual path separately. MP-VTST can be viewed as a generalization of MS-VTST. The application of MS-VTST and MP-VTST to several reactions of relevance in combustion has emphasized the importance of including multiple structures, their torsional-potential anharmonicity, and multiple paths in the calculation of rate constants.[23-24, 27, 29, 31, 33-35]

In this paper, we analyze the influence of multiple conformers and paths in the evaluation of rate constants and relative abundances of products formed in the thermal decomposition of 1-propanol radicals. As a first approximation, we study all the relevant paths of decomposition, but taking into account only the most stable stationary points (reactant and transition state) of each path. This is a one-well approximation, hereinafter referred to as 1W, which has been widely employed in theoretical calculations of rate constants. Finally, we also computed multipath (MP) rate constants, as described in the next section.

The 1-propanol radical may exist in four different isomeric species, characterized by the position from which the H-atom was abstracted or dissociated. These species are mainly formed

via H-atom abstraction by OH radicals, and the subsequent unimolecular decomposition at high temperatures is of great importance in the global combustion mechanism of 1-propanol. The ground-state PES associated with the decomposition of 1-propanol radicals was first explored in computational studies of the reaction of propene with the OH radical.[36-42] The most complete study was reported by Zádor et al.,[40] who later investigated the unimolecular dissociation of these radicals.[43] They calculated 1W rate constants as a function of pressure and temperature using a time-dependent, RRKM-based energy-resolved master equation, as implemented in the Variflex program.[44] Although most of these computational studies report very complex reaction networks, they do not show the extra complexity due to the existence of different rotameric species. The goal of this study is to assess the importance of conformations of flexible molecules (as the 1-propanol radical) in their decomposition. This issue was not investigated in the work of Zádor and Miller.[43]

COMPUTATIONAL METHODS

Finding the relevant reaction network. In the first step of this study, we performed a global, automatic search of stationary points on the ground-state PES for the unimolecular decomposition of the 1-propanol radical, using the tsscds2018 package.[45-48] This package employs the MOPAC2016 code[49] to run "on-the-fly" trajectories with a semiempirical Hamiltonian (PM7[50] in this work) and explore the surface at this level of theory. Configuration points that may be close to potential TSs are selected using the bond breaking/formation search algorithm implemented in the tsscds2018 program. Each of these TS candidates is then subjected to a geometry optimization and, if a TS is located, the program calls MOPAC2016 to perform

minimum energy path (MEP) calculations and determine the corresponding reactant and product structures. With the discovered pathways, the program constructs a reaction network. The tsscds2018 package has an interface with Gaussian 09,[51] with which the user can refine the energies of the reaction network using a high level electronic structure theory method. In this work, we employed the MPWB1K functional[52] in combination with the 6-31+G(d,p) basis set,[53-54] which is known to provide good results for thermochemical kinetics. Using the Q1 diagnostic of Lee et al.[55], Zádor et al.[40] found that a single-reference method is appropriate for the system investigated here. The dissociation of $CH_3C{\cdot}HCH_2OH$ to give propene + OH, however, may present some multireference character for configurations at which the C–O bond is broken or partially broken.

The tsscds2018 package can also compute, in an automatic fashion, thermal rate constants for all the elementary steps using standard TST, as well as the time evolution of the populations of all the chemical species involved in the reaction network, employing a kinetic Monte Carlo algorithm.[56-57] Applying these methods to the dissociation of 1-propanol radicals at a high temperature (2000 K), we selected the most relevant pathways among the whole reaction network. Specifically, we constructed a simplified reaction network by choosing the pathways resulting in at least 0.01% of product formation. For the elementary steps of this simplified reaction network, we calculated more accurate rate constants using two different approaches of VTST, as described below.

Further exploration of reactant and TS conformers. Many of the elementary reactions predicted by the tsscds2018 package involved different rotameric species of reactants and TSs. Usually, the barriers for conversion, by internal rotations, between conformers of both types of

stationary points are lower than the barriers for reaction. Because of this, we considered it convenient to define a conformational reaction channel (CRC) as the group of all the paths, including specular images, that connect the rotamers of a given reactant radical with the associated TS rotameric species.[32] In the second step of this work, and in order to ensure a thorough exploration of stationary points on the PES, for each CRC we chose a representative of the reactant and TS conformations, and we performed a systematic search for rotameric species using the Q2DTor program.[58] This program can be employed to calculate anharmonic effects due to internal rotations of the molecule,[59-60] but here we only used it to perform exploratory scans of the torsions and optimize all the other degrees of freedom for each of the points of the torsional potential. The resulting potential energy grid is fitted to a Fourier series and all the minima of this analytical PES can easily be located.

Calculation of rate constants. After this exhaustive exploration of the PES, a minimum energy path from each TS was built employing the Page-McIver method,[61] and using a stepsize of 0.005 bohr (reduced mass of 1 amu), a cubic first step and updating the Hessian every 10 steps. These electronic structure data, obtained at the MPWB1K/6-31+G(d,p) level, allowed us to evaluate thermal rate constants of each channel using the canonical variational transition state theory with multidimensional small-curvature corrections for tunneling (CVT/SCT).

For simplicity, and unless otherwise stated, all the equations of this section will refer to a given CRC. Let us denote by n_c and $n^{\ddagger}$ the numbers of distinguishable different conformations of the reactant and TS species, respectively. In this counting of distinguishable structures, we only consider one structure for a pair of enantiomers; mirror images are included separately in the definition of the multistructural partition functions as described next. Specifically, in the case of

the multistructural harmonic oscillator (MS-HO) approximation, the partition function of a set of n_{C} reactant conformers is given by:

$$Q^{\text{MS-HO}} = \sum_{i=1}^{n_{\mathrm{C}}} m_i Q_i^{\text{RRHO}} \quad (1)$$

where $m_i = 2$ if the structure of the *i*-th well in the CRC has an enantiomer, and $m_i = 1$ otherwise; Q_i^{RRHO} is the rigid-rotor, harmonic-oscillator (RRHO) partition function, that is,

$$Q_i^{\text{RRHO}} = Q_{\text{rot},i} Q_i^{\text{HO}} e^{-\beta U_i} \quad (2)$$

where $Q_{\text{rot},i}$ and Q_i^{HO} are the rigid-rotor rotational and harmonic-oscillator vibrational partition functions of (reactant) conformer *i* of a given CRC. The reactant conformers are sorted by increasing electronic energy, i.e., the conformer with the lowest electronic energy is labelled 1, whereas the one with the highest energy is labelled n_{C}. The energy of the *i*-th conformation, relative to that of the lowest energy conformer, is given by U_i; $\beta = 1/k_{\mathrm{B}}T$, where k_{B} is Boltzmann's constant and *T* the temperature. Notice that the total number of distinct reactant structures, including enantiomers, is $\sum_{i=1}^{n_{\mathrm{C}}} m_i$. The CRC may also have several transition states, in which case the corresponding multistructural partition function is given by:

$$Q^{\text{MS-HO},\ddagger} = \sum_{j=1}^{n^{\ddagger}} m_j^{\ddagger} Q_j^{\text{RRHO},\ddagger} \quad (3)$$

where $m_j^{\ddagger}$ has the same meaning as m_i but for transition states;

$$Q_j^{\text{RRHO},\ddagger} = Q_{\text{rot},j}^{\ddagger} Q_j^{\text{HO},\ddagger} e^{-\beta U_j^{\ddagger}} \quad (4)$$

$Q_{\text{rot},j}^{\ddagger}$ and $Q_j^{\text{HO},\ddagger}$ are the rigid-rotor rotational and harmonic-oscillator vibrational partition functions of the *j*-th transition state. The difference between the electronic energy of the *j*-th TS

conformer and that of the most stable TS conformer is given by $U_j^{\ddagger}$. With this prescription for the partition functions, the multistructural transition state theory (MS-TST) thermal rate constant for a given CRC reads:

$$k^{\text{MS-TST}} = B\frac{Q^{\text{MS-HO},\ddagger}}{Q^{\text{MS-HO}}} \tag{5}$$

where

$$B = \frac{1}{h\beta}\frac{Q_e^{\ddagger}}{Q_e\Phi_{\text{rel}}}e^{-\beta U^{\ddagger}} \tag{6}$$

In this equation, $Q_e^{\ddagger}$ and Q_e are the electronic partition functions of the most stable TS and reactant conformers, respectively, and h is Planck's constant. In addition, $U^{\ddagger}$ is the difference between the electronic energy of the lowest energy TS conformer and that of the lowest energy reactant conformer, and Φ_{rel} is the partition function for the relative translational motion of reactants, which is unity for unimolecular reactions. The MS-TST rate constant is a sum over the individual TST rate constants, that is,

$$k^{\text{MS-TST}} = \sum_{j=1}^{n^{\ddagger}} m_j^{\ddagger} k_j^{\text{TST}} \tag{7}$$

where

$$k_j^{\text{TST}} = B\frac{Q_j^{\text{RRHO},\ddagger}}{Q^{\text{MS-HO}}} \tag{8}$$

As in the case of reactants, subscript j sorts the transition states from the lowest to the highest energy.

The CVT/SCT thermal rate constant adds a multiplicative factor $\gamma_j^{\mathrm{CVT/SCT}}$ to the TST rate constant that accounts for variational, Γ_j^{CVT}, and tunneling, $\kappa_j^{\mathrm{CVT/SCT}}$, effects:

$$\gamma_j^{\mathrm{CVT/SCT}} = \Gamma_j^{\mathrm{CVT}} \kappa_j^{\mathrm{CVT/SCT}} \tag{9}$$

and therefore

$$k_j^{\mathrm{CVT/SCT}} = \gamma_j^{\mathrm{CVT/SCT}} k_j^{\mathrm{TST}}. \tag{10}$$

On the one hand, the evaluation of the CVT/SCT thermal rate constants involves building the MEP from each of the transition states towards reactants and products. The variational effects are given by

$$\Gamma_j^{\mathrm{CVT}} = \frac{k_j^{\mathrm{CVT}}}{k_j^{\mathrm{TST}}} \tag{11}$$

where k_j^{CVT} is the canonical variational thermal rate constant, which tries to minimize the non-recrossing assumption of TST. This assumption states that when a system reaches the dividing surface (usually defined as the plane perpendicular to the mode with imaginary frequency at the transition state), it always reacts and yields products. The variational rate constant partially corrects this assumption by positioning dividing surfaces along the MEP in such a way that the CVT rate constant is calculated at the location at which the free energy of activation has a maximum. If this maximum is located at the transition state then $\Gamma_j^{\mathrm{CVT}} = 1$, whereas $\Gamma_j^{\mathrm{CVT}} < 1$ otherwise. Therefore $k_j^{\mathrm{CVT}} \leq k_j^{\mathrm{TST}}$.

On the other hand, tunneling effects, which are included through the tunneling transmission coefficient κ, account for the probability of penetration through classically forbidden regions of the potential energy barrier. The SCT approximation collects information along the MEP to evaluate such tunneling transmission probabilities. A detailed account about how these tunneling probabilities are calculated is given elsewhere.[62-63] Notice that tunneling effects increase the thermal rate constants ($\kappa \geq 1$), whereas variational effects decrease them. At high temperatures, which are the ones of interest in combustion chemistry, tunneling effects are negligible but variational effects may be large. For temperatures lower than those considered here, a refinement in the calculations of the tunneling transmission factors may be needed. Two accurate approximations for taking tunneling into account at low temperatures are the least-action path method[64-65] and the microcanonically optimized multidimensional tunneling method.[66] In the latter approximation, at every tunneling temperature, the tunneling probability is taken as the maximum between the small-curvature and the large-curvature tunneling probabilities.[67-68]

Additionally, it is important to clarify that MS-TST and MP-TST refer to the same thermal rate constants. However, it is more adequate to use the term MS-TST than MP-TST because in TST the rate constants are independent of the path that the system follows to reach the transition state. This is not the case in VTST, in which the definition of one (MS-VTST) or several (MP-VTST) paths needs to be specified in order to calculate the corrections to the TST assumptions.

The expression for the MP-CVT/SCT thermal rate constant is similar to the expression for MS-TST but including the tunneling and variational effects, i.e.,

$$k^{\text{MP-CVT/SCT}} = \sum_{j=1}^{n^{\ddagger}} m_j^{\ddagger} k_j^{\text{CVT/SCT}} = \sum_{j}^{n^{\ddagger}} \gamma_j^{\text{CVT/SCT}} m_j^{\ddagger} k_j^{\text{TST}} \qquad (12)$$

A different, but equivalent, way to write eq 12 is:

$$k^{\text{MP-CVT/SCT}} = \langle \gamma^{\text{CVT/SCT}} \rangle \sum_{j=1}^{n^{\ddagger}} m_j^{\ddagger} k_j^{\text{TST}} = \langle \gamma^{\text{CVT/SCT}} \rangle k^{\text{MS-TST}} \tag{13}$$

where $\langle \gamma^{\text{CVT/SCT}} \rangle$ is the average of variational and tunneling effects for the CRC. It is given by:

$$\langle \gamma^{\text{CVT/SCT}} \rangle = \frac{\sum_{j=1}^{n^{\ddagger}} \gamma_j^{\text{CVT/SCT}} m_j^{\ddagger} Q_j^{\text{RRHO},\ddagger}}{Q^{\text{MS-HO},\ddagger}} \tag{14}$$

Notice that in eq 14 $\langle \gamma^{\text{CVT/SCT}} \rangle$ is independent of the reactant properties. If we assume that the variational and tunneling effects obtained from the MEP starting from the transition state with the lowest energy are representative of these effects in the whole CRC ($\langle \gamma^{\text{CVT/SCT}} \rangle = \gamma_1^{\text{CVT/SCT}}$), then we have the MS-CVT/SCT thermal rate constant, which is given by:

$$Q^{\text{MS-CVT/SCT}} = \gamma_1^{\text{CVT/SCT}} \sum_{j=1}^{n_k^{\ddagger}} m_j^{\ddagger} k_j^{\text{TST}} = \gamma_1^{\text{CVT/SCT}} k^{\text{MS-TST}} \tag{15}$$

In the case of 1W-TST and 1W-CVT/SCT the sums in eqs 7, 12-15 are reduced to one term (i.e., to structure 1 in both reactants and transition states) and with $m_1 = m_1^{\ddagger} = 1$. Thus:

$$k^{\text{1W-TST}} = B \frac{Q_1^{\text{RRHO},\ddagger}}{Q_1^{\text{RRHO}}} \tag{16}$$

and

$$k^{\text{1W-CVT/SCT}} = \gamma_1^{\text{CVT/SCT}} k^{\text{1W-TST}} \tag{17}$$

In this work, CVT/SCT rate constants were calculated for temperatures ranging from 1000 to 2000 K, and using the MP and the 1W approaches given by eqs 12 and 17, respectively. The calculations were carried out with our own code (TheRa program), utilizing energies and

derivatives obtained by using an interface with the Gaussian 09 package.[51] Finally, the populations of all the chemical species as a function of time were computed using a kinetic Monte Carlo (KMC) algorithm based on Gillespie's direct method.[56-57] These KMC simulations assume the reactions behave statistically over the whole decomposition process.

RESULTS AND DISCUSSION

As mentioned in the previous section, we used the tsscds2018 package[45-47] to predict reaction pathways on the C_3H_7O potential energy surface. Employing the PM7 Hamiltonian[50] for the trajectories and the MPWB1K functional[52] together with the 6-31+G(d,p) basis set for the high-level electronic structure calculations, we found more than one thousand transition states. Using standard transition state theory and a kinetic Monte Carlo simulation at 2000 K, we obtained 15 relevant conformational reaction channels (CRCs). These channels are depicted in Figure 1, which also includes molecular drawings for the most stable conformations of the reactants and transition states. For clarity, these molecular drawings are presented separately in Figure 2. For completeness, we also included in our study the dissociation of the CH_3CHCH_2OH radical into propene + OH (CRC16), which has no saddle point at the MPWB1K/6-31+G(d,p) level. For this CRC we used a distinguished reaction coordinate (the C_α–O distance) to locate the variational transition state. The channels presented in Figure 1 coincide with the relevant channels reported by Zádor et al.,[40] which were selected to study the terminal addition of the OH radical to propene (Fig. 1 in their paper) and, later, the unimolecular dissociation of propanol radicals.[43] We notice that there is a mistake in the energetic profiles reported in the former paper of Zádor at al.,[40] specifically, the dissociation channels occurring from radicals CH_2CH_2CHOH and CH_3CH_2CHO are interchanged. As can be shown from inspection of Figure 1, all the minima

are interconnected via H-migration reactions, which present very high barriers, and so, in general, they will not be the preferred paths.

All the relevant CRCs are also gathered in Table 1, which specifies the nomenclature used in this paper for the minima and transition states. In particular, minimum structures are named using the acronym PrOH followed by the symbol of the atom from which the hydrogen was abstracted or dissociated from 1-propanol to give the radical. The Greek letters α, β and γ specify the position of the radical carbon atom (C_α is the first C atom attached to the functional group, C_β the second and C_γ the third one). Notice that we have split channels CRC04 and CRC08 into *cis* and *trans* pathways. These channels lead to *cis*- and *trans*-1-propenol, and therefore there are 18 CRCs in total. In the table, lowercase italic letters *c* and *t* are employed to distinguish *cis* and *trans* arrangements. For CRCs leading to dissociation, we did not consider, in our analyses, the backward reactions, that is, the association processes.

Table 2 shows the number of different conformers, without the inclusion of enantiomers, found in this work for the minima and transition states. We notice that using the Q2DTor program we found a few conformers not discovered in the exploration of the PES conducted by the tsscds2018 program. For each family of conformers, the relative energy of the lowest-energy rotamer is presented in the table. These relative energies include zero-point vibrational energy (ZPE) contributions. The geometries, energies, vibrational frequencies and enantiomer numbers for all the stationary points considered in this study are detailed in the Supporting Information (SI). It is remarkable that most reactant species and some transition structures have many different rotamers. For example, the H–Cγ dissociation from PrOH_C_β to give allyl alcohol (CRC11) involves four different reactant conformers and nine TS structures. The same

conformation numbers are present in CRC13 (forward reaction), which is the H-migration interconversion channel between PrOH_C_β and PrOH_C_γ. For the backward reaction, the reactant radical (PrOH_C_γ) exhibits five different rotamers. Additionally, it is remarkable the H–C_β dissociation from PrOH_C_γ (CRC15), which also leads to allyl alcohol, as CRC11, via a TS family of nine rotamers.

As already mentioned, the most detailed C_3H_7O PES reported previously is that of Zádor et al.[40,43] They performed B3LYP/6-311++G(d,p) computations for geometry optimizations and frequency evaluations, as well as subsequent single-point calculations using the QCISD(T) method with the cc-pV*n*Z basis sets, *n* = (T, Q), for extrapolation to the complete basis set limit cc-pV∞Z.[69-70] For their reaction network, they only considered the most stable conformers of reactants and transition states. The MPWB1K/6-31+G(d,p) level employed in the present study is not as accurate, but it gives a good compromise between accuracy and cost,[52] taking into account the large number of MEP calculations needed to compute the reaction network and the rate constants. A comparison between the relative energies listed in Table 2 and those reported by Zádor et al. gives a root-mean-square deviation of 0.9 kcal/mol. However, for several structures we found significant discrepancies. For example, our relative energy for the most stable conformer of the PrOH_O radical is about 4 kcal/mol smaller than their result. Also, the relative energies of the most stable conformers of TS11 and TS15 are 4 kcal/mol larger than in their study. Unfortunately, their work does not provide information about the geometries of the optimized structures, so that the relative energies used for the comparison might not correspond to the same conformations.

As pointed out in the previous section, enantiomerism may play a significant role in the calculation of MP rate constants. Almost all the reactant conformers of 1-propanol radicals have conformational enantiomers, that is, nonsuperimposable mirror images of one another that can be interconverted by internal rotations about single bonds.[71] The only exception we found in this work corresponds to the all-anti conformation of PrOH_O, which is not the lowest energy conformer of this radical. In the same way, all the TS conformers exhibit enantiomerism, except the all-anti conformer of TS01 (TS01-02 structure in the SI). However, for TSs, many of the enantiomers are configurational, namely, nonsuperimposable mirror images of each other that can be interconverted only by breaking and forming bonds.[71] For the system that is being investigated in this study, since $m_i = m_j^{\ddagger} = 2$, except for the two conformers specified above, enantiomerism does not have a significant influence on the calculated rate constants, because the contributions from the TSs are cancelled out by those from the reactants.

Using the 1W and MP approaches described in the previous section, we calculated rate constants for the CRCs at a series of temperatures ranging from 1000 to 2000 K in steps of 50 K. The rate constants of the backward reactions of the CRCs leading to isomerization of the radical were obtained using the principle of detailed balance and the equilibrium constants. The values computed at 1500 K are shown in Table 3; values calculated at 1000 and 2000 K are reported in the SI. As can be seen, depending on the channel, there are significant differences between the rate constants calculated with the two approaches. To facilitate the comparison, we include in the table the values calculated for the 1W/MP ratio. In addition, the last entry of the table gives the quotient between the number of TS conformers and that of the reactant species, $n^{\ddagger}/n_c$. Finally, we have also included in Table 3 the rate constants calculated at 1500 K using the expression $AT^n\exp(-E/(RT))$ and the A, n and E parameters reported by Zádor and Miller,[43] corresponding to the high-pressure

limit. As mentioned before, they calculated 1W rate constants with the Variflex program,[44] using an RRKM-based master equation. As could be anticipated from the differences between our energetic profiles and those reported by Zádor et al.,[40,43] we found substantial discrepancies between the two sets of 1W rate constants. For several channels, the differences are of one order of magnitude. For the dissociation of PrOH_C_β into allyl alcohol + H, their rate constant is two orders of magnitude smaller than ours. This result is very striking since the energy barrier calculated here for this channel is about 4 kcal/mol larger than that reported in their study.

It is difficult to extract significant conclusions from the previous comparison because the two sets of rate constants were obtained with data calculated using different levels of electronic structure theory and different reaction-rate methods. However, the aim of this work is to assess the importance of conformations and paths in the calculation of rate constants and product abundances, and therefore the relevant comparison is that between our 1W and MP results. On the basis of multistructural TST, we may expect a rough correlation between the $n^{\ddagger}/n_c$ and the 1W/MP ratios. For example, CRC01, for which we obtained a ratio close to unity, has two different conformers for both the reactant and TS. If we disregard variational effects, the contribution from the second reactant conformer to the multistructural partition function, given by eq 1, is approximately counterbalanced by the contribution from the second TS conformer to the TS multistructural partition function (eq 3). Small $n^{\ddagger}/n_c$ ratios will lead to a significant decrease of the MP rate constant in comparison with the 1W value. Thus, the MP rate constant calculated for the backward reaction of the CRC07 channel ($n^{\ddagger}/n_c = 1/5$) is about six times smaller than the 1W one. On the other hand, the MP rate constants computed for CRCs having $n^{\ddagger}/n_c$ ratios around 2 (e.g., CRC11, CRC13 and CRC15) are about twice the corresponding 1W rate constants. Of course, structural factors of the different conformers, such as relative energies and vibrational frequencies, and variational effects

also affect the 1W/MP ratios, thus making the above correlation only acceptable from a qualitative point of view. As indicated in the previous section, at the temperatures selected for the calculations, tunneling is expected to be negligible.

We performed kinetic Monte Carlo simulations to predict the populations of the 1-propanol radicals and products as a function of time, and to compute product branching ratios. For each temperature and set of rate constants (i.e., 1W and MP), we carried out four independent simulations, starting each of them from one of the four radicals. Figure 3 shows graphically the product branching ratios, as a function of temperature, obtained from simulations initiated at the PrOH_O radical. The branching ratios were calculated as $100 \times N/N_{R,0}$, were N is the number of molecules of a particular product and $N_{R,0}$ is the total number of reactant molecules at zero time (i.e., at the beginning of the simulation). As shown in Figure 3, both the 1W and the MP approaches provide quite similar results. The most abundant product is formaldehyde + ethyl radical, which is formed by direct dissociation via CRC01. This result could be anticipated because this channel has, by far, the largest rate constant among the five competing reactions that share PrOH_O as reactant. As expected, the increase in the temperature facilitates the decomposition of the radical through alternative routes, specifically, via direct H–C_α scission to give propanal (CRC05).

When the KMC simulations are initiated at the PrOH_C_α radical, we obtained the product branching ratios depicted in Figure 4. From a qualitative point of view, the simulations give similar trends, although quantitatively there are significant deviations between the 1W and MP predictions. As expected, and considering the values of the rate constants for the competing channels associated with the PrOH_C_α reactant, direct dissociation to give vinyl alcohol and a

methyl radical (CRC02) is the dominant process. The importance of this channel slightly decreases with the temperature, mainly at the expense of propanal formation via direct H–C_α dissociation (CRC03).

The product branching ratios obtained from KMC simulations starting from the PrOH_C_β radical are shown in Figure 5. In this case, the kinetics are dominated by the barrierless dissociation leading to propene + OH (CRC16). As the temperature increases, the importance of this CRC decreases, especially in the KMC simulations run with the MP rate constants, and other pathways start to contribute to the total decomposition, mainly direct H–C_α scissions to give *cis*- and *trans*-1-propenol (*c*-CRC08 and *t*-CRC08, respectively). At the highest temperatures, the simulations performed with the MP rate constants also predict significant formation of allyl alcohol via direct H–C_γ dissociation (CRC11). By contrast, the branching ratio of allyl alcohol calculated with the 1W rate constants is negligible.

The KMC simulations initiated at the PrOH_C_γ radical predict the product branching ratios displayed in Figure 6. At the lowest temperature investigated, the differences between the MP and the 1W ratios are considerable. The simulations carried out with the MP rate constants predict that formation of ethene and hydroxymethyl radical (CH_2OH), through direct C_α–C_β scission (CRC06), is the dominant pathway, followed by production of formaldehyde and ethyl radical. The latter process involves isomerization to PrOH_O and the consecutive reaction CRC01. The 1W product ratios, however, displays a different picture, as the abundance of formaldehyde and ethyl radical is slightly higher than that of ethene and CH_2OH. To understand how the kinetics of CH_2O + CH_2CH_3 formation takes place, let us analyze the ratios of the four reactant radicals obtained from a KMC simulation performed at 1000 K. The ratios obtained

using the 1W rate constants, listed in Table S1 (see the SI), are plotted as a function of time in Figure 7 (the MP ratios show similar behavior). As can be seen, the ratios of the intermediate radicals, and particularly that of PrOH_O, are negligible. However, this radical plays a crucial role, as it is acting as a fleeting intermediate that canalizes, via CRC01, a large fraction of the radical decomposition. In fact, for PrOH_C_γ as a reactant and at 1000 K, the largest rate constant calculated with the 1W approach corresponds to isomerization to PrOH_O via CRC07 (backward direction), followed by direct dissociation through CRC06 to give ethene + CH_2OH (see Table S1 and Figure 1). Now, for PrOH_O, the C_α–C_β dissociation leading to CH_2O + CH_2CH_3 (CRC01) completely prevails over its competing channels. Notice that, at 1000 K, its rate constant is two orders of magnitude larger than that of CRC06. Therefore, even for very small ratios of the PrOH_O intermediate, the propensity[57] or stochastic rate (i.e., the rate constant multiplied by the number of the corresponding reactant molecules) of the CRC01 channel may be larger than that of CRC06. As a result, formation of CH_2O + CH_2CH_3 becomes the most favorable decomposition process. For the MP approach, the rate constant of the CRC06 path is twice that of backward CRC07 (at 1000 K), thus resulting in higher production of ethene + CH_2OH.

Continuing with the discussion of the KMC simulations initiated at the PrOH_C_γ radical, it can be seen that, as the temperature increases, the KMC simulations carried out with the 1W and MP sets of rate constants lead to rather similar trends, although quantitatively there are significant differences between the 1W and MP branching ratios. All these results point out that the neglect of contributions from the different conformers of reactants and transition states may result in significant errors in the calculation of rate constants, which reinforces the conclusions of recent studies,[23-24,28-29,31] and in turn in the evaluation of product branching ratios.

CONCLUSIONS

Using automated codes, we have performed an exhaustive exploration of the potential energy surface associated with the unimolecular decomposition of 1-propanol radicals, and determined the reaction network relevant for the range of temperatures considered in this work. The simplified network shown in Figure 1 comprises all the relevant paths previously reported by Zádor et al.[40] Their whole network, however, does not display the wealth of conformational paths described in the present study.

We have investigated the role of multiple reactant and TS conformers on the rate constants and product branching ratios in the decomposition of 1-propanol radicals. Thermal rate constants for all the elementary reactions were evaluated using two different approaches in the framework of VTST. In the simplest approach (1W), only the most stable conformer of the reactant and that of the transition state were considered in the calculations. The second approach includes contributions from all the conformers using the multipath formulation. The results clearly indicate that, in cases where reactants and transition states exhibit various rotamers, the neglect of contributions from the additional stationary points may result in large errors in the calculation of rate constants and product branching ratios.

Finally, the present study encourages the use of automated methods for discovering reaction pathways and predicting complex reaction mechanisms. We are entering a new era in chemical kinetics and dynamics, where automated codes will extraordinarily facilitate the hard and tedious work of exploring complex reactions. In future work, we plan to interface the tsscds2018 package with the Q2DTor and the TheRa programs, in such a way that researchers in

the field of chemical kinetics and dynamics will be able to routinely use them to predict reaction mechanisms and to easily perform computer simulations of gas-phase complex reactions.

ASSOCIATED CONTENT

Supporting Information. Geometries, electronic energies, frequencies and drawings of all the relevant stationary points considered in this study are gathered in the Supporting Information (PDF).

AUTHOR INFORMATION

Corresponding Authors

*D. Ferro-Costas. E-mail: david.ferro@usc.es

*A. Fernández-Ramos: qf.ramos@usc.es

*S. A. Vázquez: saulo.vazquez@usc.es

Author Contributions

The manuscript was written through contributions of all authors. All authors have given approval to the final version of the manuscript.

Funding Sources

This work was partially supported by the Consellería de Cultura, Educación e Ordenación Universitaria e da Consellería de Economía, Emprego e Industria (Axuda para Consolidación e

Estructuración de unidades de investigación competitivas do Sistema Universitario de Galicia, Xunta de Galicia ED431C 2017/17 & Centro singular de investigación de Galicia acreditación 2016-2019, ED431G/09), the Ministerio de Economía y Competitividad of Spain (Research Grant No CTQ2014-58617-R) and the European Regional Development Fund (ERDF). D. F.-C. also thanks Xunta de Galicia for financial support through a postdoctoral grant.

Notes

The authors declare no competing financial interest.

ACKNOWLEDGMENT

The authors thank "Centro de Supercomputación de Galicia (CESGA)" for the use of their computational facilities.

ABBREVIATIONS

TS, transition state; TST, transition state theory; VTST, variational TST; MS, multistructural; MP, multipath; CVT, canonical variational transition state theory; SCT, multidimensional small-curvature corrections for tunneling; CRC, conformational reaction channel.

REFERENCES

1. MacLean, H. L.; Lave, L. B., Evaluating automobile fuel/propulsion system technologies. *Prog. Energy Combust. Sci.* **2003,** *29* (1), 1-69.
2. Balat, M.; Balat, H.; Öz, C., Progress in bioethanol processing. *Prog. Energy Combust. Sci.* **2008,** *34* (5), 551-573.
3. Service, R. F., Biofuel Researchers Prepare to Reap a New Harvest. *Science* **2007,** *315* (5818), 1488-1491.
4. Chen, H.; Shi-Jin, S.; Jian-Xin, W., Study on combustion characteristics and PM emission of diesel engines using ester–ethanol–diesel blended fuels. *Proceedings of the Combustion Institute* **2007,** *31* (2), 2981-2989.
5. Jacobson, M. Z., Effects of Ethanol (E85) versus Gasoline Vehicles on Cancer and Mortality in the United States. *Environmental Science & Technology* **2007,** *41* (11), 4150-4157.
6. Agarwal, A. K., Biofuels (alcohols and biodiesel) applications as fuels for internal combustion engines. *Prog. Energy Combust. Sci.* **2007,** *33* (3), 233-271.
7. Holtzapple, M. T.; Davison, R. R.; Ross, M. K.; Aldrett-Lee, S.; Nagwani, M.; Lee, C.-M.; Lee, C.; Adelson, S.; Kaar, W.; Gaskin, D.; Shirage, H.; Chang, N.-S.; Chang, V. S.; Loescher, M. E., Biomass conversion to mixed alcohol fuels using the MixAlco process. *Appl. Biochem. Biotechnol.* **1999,** *79* (1), 609-631.
8. Atsumi, S.; Liao, J. C., Directed Evolution of Methanococcus jannaschii Citramalate Synthase for Biosynthesis of 1-Propanol and 1-Butanol by Escherichia coli. *Appl. Environ. Microbiol.* **2008,** *74* (24), 7802-7808.
9. Shen, C. R.; Liao, J. C., Metabolic engineering of Escherichia coli for 1-butanol and 1-propanol production via the keto-acid pathways. *Metab. Eng.* **2008,** *10* (6), 312-320.
10. Barnard, J. A.; Hughes, H. W. D., The pyrolysis of n-propanol. *Transactions of the Faraday Society* **1960,** *56* (0), 64-71.
11. Barnard, J. A., The pyrolysis of isopropanol. *Transactions of the Faraday Society* **1960,** *56* (0), 72-79.
12. Kasper, T.; Oßwald, P.; Struckmeier, U.; Kohse-Höinghaus, K.; Taatjes, C. A.; Wang, J.; Cool, T. A.; Law, M. E.; Morel, A.; Westmoreland, P. R., Combustion chemistry of the propanol isomers — investigated by electron ionization and VUV-photoionization molecular-beam mass spectrometry. *Combustion and Flame* **2009,** *156* (6), 1181-1201.
13. Frassoldati, A.; Cuoci, A.; Faravelli, T.; Niemann, U.; Ranzi, E.; Seiser, R.; Seshadri, K., An experimental and kinetic modeling study of n-propanol and iso-propanol combustion. *Combustion and Flame* **2010,** *157* (1), 2-16.
14. Kohse-Höinghaus, K.; Oßwald, P.; Cool, T. A.; Kasper, T.; Hansen, N.; Qi, F.; Westbrook, C. K.; Westmoreland, P. R., Biofuel Combustion Chemistry: From Ethanol to Biodiesel. *Angew. Chem. Int. Ed.* **2010,** *49* (21), 3572-3597.
15. Man, X.; Tang, C.; Zhang, J.; Zhang, Y.; Pan, L.; Huang, Z.; Law, C. K., An experimental and kinetic modeling study of n-propanol and i-propanol ignition at high temperatures. *Combustion and Flame* **2014,** *161* (3), 644-656.
16. Sarathy, S. M.; Oßwald, P.; Hansen, N.; Kohse-Höinghaus, K., Alcohol combustion chemistry. *Prog. Energy Combust. Sci.* **2014,** *44* (Supplement C), 40-102.
17. Yang, K.; Zhan, C.; Man, X.; Guan, L.; Huang, Z.; Tang, C., Shock Tube Study on Propanal Ignition and the Comparison to Propane, n-Propanol, and i-Propanol. *Energy & Fuels* **2016,** *30* (1), 717-724.

18. Jouzdani, S.; Zhou, A.; Akih-Kumgeh, B., Propanol isomers: Investigation of ignition and pyrolysis time scales. *Combustion and Flame* **2017,** *176* (Supplement C), 229-244.
19. Glassman, I.; Yetter, R. A.; Glumac, N. G., *Combustion*. 5th ed.; Academic Press, Elsevier: 2015.
20. Truhlar, D. G.; Isaacson, A. D.; Garret, G. C., *In Theory of Chemical Reaction Dynamics*. Baer, M., CRC: Boca Raton, FL: 1985; Vol. 4, p. 65.
21. Fernández-Ramos, A.; Ellingson, A.; Garrett, B. C.; Truhlar, D. G., Variational Transition State Theory with Multidimensional Tunneling. *Rev. Comput. Chem.* **2007,** *23*, 125-232.
22. Bao, J. L.; Truhlar, D. G., Variational transition state theory: theoretical framework and recent developments. *Chemical Society Reviews* **2017,** *46* (24), 7548-7596.
23. Yu, T.; Zheng, J.; Truhlar, D. G., Multi-structural variational transition state theory. Kinetics of the 1,4-hydrogen shift isomerization of the pentyl radical with torsional anharmonicity. *Chem. Sci.* **2011,** *2* (11), 2199-2213.
24. Xu, X.; Yu, T.; Papajak, E.; Truhlar, D. G., Multistructural Variational Transition State Theory: Kinetics of the Hydrogen Abstraction from Carbon-2 of 2-Methyl-1-propanol by Hydroperoxyl Radical Including All Structures and Torsional Anharmonicity. *J. Phys. Chem. A* **2012,** *116* (43), 10480-10487.
25. Zheng, J.; Truhlar, D. G., Multi-path variational transition state theory for chemical reaction rates of complex polyatomic species: ethanol + OH reactions. *Faraday Discussions* **2012,** *157* (0), 59-88.
26. Zheng, J.; Truhlar, D. G., Quantum Thermochemistry: Multistructural Method with Torsional Anharmonicity Based on a Coupled Torsional Potential. *J. Chem. Theory Comput.* **2013,** *9* (3), 1356-1367.
27. Bao, J. L.; Xing, L.; Truhlar, D. G., Dual-Level Method for Estimating Multistructural Partition Functions with Torsional Anharmonicity. *J. Chem. Theory Comput.* **2017,** *13* (6), 2511-2522.
28. Meana-Pañeda, R.; Fernández-Ramos, A., Tunneling and Conformational Flexibility Play Critical Roles in the Isomerization Mechanism of Vitamin D. *J. Am. Chem. Soc.* **2012,** *134* (1), 346-354.
29. Bao, J. L.; Meana-Paneda, R.; Truhlar, D. G., Multi-path variational transition state theory for chiral molecules: the site-dependent kinetics for abstraction of hydrogen from 2-butanol by hydroperoxyl radical, analysis of hydrogen bonding in the transition state, and dramatic temperature dependence of the activation energy. *Chem. Sci.* **2015,** *6* (10), 5866-5881.
30. Simón-Carballido, L.; Alves, T. V.; Dybala-Defratyka, A.; Fernández-Ramos, A., Kinetic Isotope Effects in Multipath VTST: Application to a Hydrogen Abstraction Reaction. *J. Chem. Phys. B* **2016,** *120* (8), 1911-1918.
31. Bao, J. L.; Sripa, P.; Truhlar, D. G., Path-dependent variational effects and multidimensional tunneling in multi-path variational transition state theory: rate constants calculated for the reactions of HO2 with tert-butanol by including all 46 paths for abstraction at C and all six paths for abstraction at O. *Phys. Chem. Chem. Phys.* **2016,** *18* (2), 1032-1041.
32. Meana-Pañeda, R.; Fernández-Ramos, A., Accounting for conformational flexibility and torsional anharmonicity in the H + CH3CH2OH hydrogen abstraction reactions: A multi-path variational transition state theory study. *J. Chem. Phys.* **2014,** *140* (17), 174303.

33. Yu, T.; Zheng, J.; Truhlar, D. G., Multipath Variational Transition State Theory: Rate Constant of the 1,4-Hydrogen Shift Isomerization of the 2-Cyclohexylethyl Radical. *J. Phys. Chem. A* **2012,** *116* (1), 297-308.
34. Xing, L.; Bao, J. L.; Wang, Z.; Zhang, F.; Truhlar, D. G., Degradation of Carbonyl Hydroperoxides in the Atmosphere and in Combustion. *J. Am. Chem. Soc.* **2017,** *139* (44), 15821-15835.
35. Simón-Carballido, L.; Bao, J. L.; Alves, T. V.; Meana-Pañeda, R.; Truhlar, D. G.; Fernández-Ramos, A., Anharmonicity of Coupled Torsions: The Extended Two-Dimensional Torsion Method and Its Use To Assess More Approximate Methods. *J. Chem. Theory Comput.* **2017,** *13* (8), 3478-3492.
36. Alvarez-Idaboy, J. R.; Díaz-Acosta, I.; Vivier-Bunge, A., Energetics of Mechanism of OH-Propene Reaction at Low Pressures in Inert Atmosphere. *J. Comp. Chem.* **1998,** *19*, 881-819.
37. Díaz-Acosta, I.; Alvarez-Idaboy, J. R.; Vivier-Bunge, A., Mechanism of the OH–propene–O_2 reaction: An ab initio study. *International Journal of Chemical Kinetics* **1999,** *31* (1), 29-36.
38. Szori, M.; Fittschen, C.; Csizmadia, I. G.; Viskolcz, B., Allylic H-Abstraction Mechanism: The Potential Energy Surface of the Reaction of Propene with OH Radical. *J. Chem. Theory Comput.* **2006,** *2* (6), 1575-1586.
39. El-Nahas, A. M.; Uchimaru, T.; Sugie, M.; Tokuhashi, K.; Sekiya, A., Relative reactivity and regioselectivity of halogen-substituted ethenes and propene toward addition of an OH radical or O (3P) atom: An ab initio study. *J. Mol. Struct. (THEOCHEM)* **2006,** *770* (1), 59-65.
40. Zádor, J.; Jasper, A. W.; Miller, J. A., The reaction between propene and hydroxyl. *Phys. Chem. Chem. Phys.* **2009,** *11* (46), 11040-11053.
41. Zhou, C.-W.; Li, Z.-R.; Li, X.-Y., Kinetics and Mechanism for Formation of Enols in Reaction of Hydroxide Radical with Propene. *J. Phys. Chem. A* **2009,** *113* (11), 2372-2382.
42. Huynh, L. K.; Zhang, H. R.; Zhang, S.; Eddings, E.; Sarofim, A.; Law, M. E.; Westmoreland, P. R.; Truong, T. N., Kinetics of Enol Formation from Reaction of OH with Propene. *J. Phys. Chem. A* **2009,** *113* (13), 3177-3185.
43. Zádor, J.; Miller, J. A., Unimolecular dissociation of hydroxypropyl and propoxy radicals. *Proceedings of the Combustion Institute* **2013,** *34* (1), 519-526.
44. Klippenstein, S. J.; Wagner, A. F.; Dunbar, R. C.; Wardlaw, D. M.; Roberston, S. H.; Miller, J. A. *VARIFLEX, 2.03m ed.*, 2011.
45. Martinez-Nunez, E., An automated transition state search using classical trajectories initialized at multiple minima. *Phys. Chem. Chem. Phys.* **2015,** *17* (22), 14912-14921.
46. Martínez-Núñez, E., An automated method to find transition states using chemical dynamics simulations. *J. Comp. Chem.* **2015,** *36* (4), 222-234.
47. Varela, J. A.; Vazquez, S. A.; Martinez-Nunez, E., An automated method to find reaction mechanisms and solve the kinetics in organometallic catalysis. *Chem. Sci.* **2017,** *8* (5), 3843-3851.
48. Rodríguez, A.; Rodríguez-Fernández, R.; Vázquez, S. A.; Barnes;, G. L.; Stewart, J. J. P.; Martínez-Núñez, E., tsscds2018: a code for automated discovery of chemical reaction mechanisms and solving the kinetics. *J. Comp. Chem.*, submitted to publication. The program can be downloaded from http://forge.cesga.es/projects/tsscds.
49. Stewart, J. J. P. *MOPAC2016*, 16.307; Steward Computational Chemistry, web-site: http://OpenMOPAC.net: 2016.

50. Stewart, J. J. P., Optimization of parameters for semiempirical methods VI: more modifications to the NDDO approximations and re-optimization of parameters. *J. Mol. Model.* **2013,** *19* (1), 1-32.
51. Frisch, M. J.; Trucks, G. W.; Schlegel, H. B. S., G. E.; Robb, M. A.; Cheeseman, J. R.; Scalmani, G.; Barone, V.; Mennucci, B.; Petersson, G. A.; Nakatsuji, H.; Caricato, M.; Li, X.; Hratchian, H. P.; Izmaylov, A. F.; Bloino, J.; Zheng, G.; Sonnenberg, J. L.; Hada, M.; Ehara, M.; Toyota, K.; Fukuda, R.; Hasegawa, J.; Ishida, M.; Nakajima, T.; Honda, Y.; Kitao, O.; Nakai, H.; Vreven, T.; Montgomery, Jr., J. A.; Peralta, J. E.; Ogliaro, F.; Bearpark, M.; Heyd, J. J.; Brothers, E.; Kudin, K. N.; Staroverov, V. N.; Kobayashi, R.; Normand, J.; Raghavachari, K.; Rendell, A.; Burant, J. C.; Iyengar, S. S.; Tomasi, J.; Cossi, M.; Rega, N.; Millam, J. M.; Klene, M.; Knox, J. E.; Cross, J. B.; Bakken, V.; Adamo, C.; Jaramillo, J.; Gomperts, R.; Stratmann, R. E.; Yazyev, O.; Austin, A. J.; Cammi, R.; Pomelli, C.; Ochterski, J. W.; Martin, R. L.; Morokuma, K.; Zakrzewski, V. G.; Voth, G. A.; Salvador, P.; Dannenberg, J. J.; Dapprich, S.; Daniels, A. D.; Farkas, Ö.; Foresman, J. B.; Ortiz, J. V.; Cioslowski, J.; Fox, D. J. *Gaussian 09, revision B.01*, Gaussian, Inc.: Wallingford CT: 2009.
52. Zhao, Y.; Truhlar, D. G., Hybrid Meta Density Functional Theory Methods for Thermochemistry, Thermochemical Kinetics, and Noncovalent Interactions: The MPW1B95 and MPWB1K Models and Comparative Assessments for Hydrogen Bonding and van der Waals Interactions. *J. Phys. Chem. A* **2004,** *108* (33), 6908-6918.
53. Hehre, W. J.; Ditchfield, R.; Pople, J. A., Self—Consistent Molecular Orbital Methods. XII. Further Extensions of Gaussian—Type Basis Sets for Use in Molecular Orbital Studies of Organic Molecules. *J. Chem. Phys.* **1972,** *56* (5), 2257-2261.
54. Hehre, W. J.; Radom, L.; Schleyer, P. v. R.; Pople, J. A., *Ab Initio Molecular Orbital Theory*. 1st ed.; Wiley: New York, 1986.
55. Lee, T. J.; Rendell, A. P.; Taylor, P. R., Comparison of the quadratic configuration interaction and coupled-cluster approaches to electron correlation including the effect of triple excitations. *J. Chem. Phys.* **1990,** *94* (14), 5463-5468.
56. Gillespie, D. T., A general method for numerically simulating the stochastic time evolution of coupled chemical reactions. *J. Comput. Phys.* **1976,** *22* (4), 403-434.
57. Gillespie, D. T., Stochastic Simulation of Chemical Kinetics. *Annu. Rev. Phys. Chem.* **2007,** *58* (1), 35-55.
58. Ferro-Costas, D.; Cordeiro, M. N. D. S.; Truhlar, D. G.; Fernández-Ramos, A., Q2DTor: A Program to Treat Torsional Anharmonicity Through Coupled Pair Torsions in Flexible Molecules. *Comput. Phys. Commun.*, (submitted).
59. Fernández-Ramos, A., Accurate treatment of two-dimensional non-separable hindered internal rotors. *J. Chem. Phys.* **2013,** *138* (13), 134112.
60. Simón-Carballido, L.; Fernández-Ramos, A., Calculation of the two-dimensional non-separable partition function for two molecular systems. *J. Mol. Model.* **2014,** *20* (4), 2190.
61. Page, M.; Jr., J. W. M., On evaluating the reaction path Hamiltonian. *J. Chem. Phys.* **1988,** *88* (2), 922-935.
62. Liu, Y. P.; Lynch, G. C.; Truong, T. N.; Lu, D. H.; Truhlar, D. G.; Garrett, B. C., Molecular modeling of the kinetic isotope effect for the [1,5]-sigmatropic rearrangement of cis-1,3-pentadiene. *J. Am. Chem. Soc.* **1993,** *115* (6), 2408-2415.
63. Lu, D.-h.; Truong, T. N.; Melissas, V. S.; Lynch, G. C.; Liu, Y.-P.; Garrett, B. C.; Steckler, R.; Isaacson, A. D.; Rai, S. N.; Hancock, G. C.; Lauderdale, J. G.; Joseph, T.; Truhlar,

D. G., POLYRATE 4: A new version of a computer program for the calculation of chemical reaction rates for polyatomics. *Comput. Phys. Commun.* **1992,** *71* (3), 235-262.
64. Garrett, B. C.; Truhlar, D. G., A least-action variational method for calculating multidimensional tunneling probabilities for chemical reactions. *J. Chem. Phys.* **1983,** *79* (10), 4931-4938.
65. Meana-Pañeda, R.; Truhlar, D. G.; Fernández-Ramos, A., Least-Action Tunneling Transmission Coefficient for Polyatomic Reactions. *J. Chem. Theory Comput.* **2010,** *6* (1), 6-17.
66. Liu, Y. P.; Lu, D. H.; Gonzalez-Lafont, A.; Truhlar, D. G.; Garrett, B. C., Direct dynamics calculation of the kinetic isotope effect for an organic hydrogen-transfer reaction, including corner-cutting tunneling in 21 dimensions. *J. Am. Chem. Soc.* **1993,** *115* (17), 7806-7817.
67. Fernandez-Ramos, A.; Truhlar, D. G., Improved algorithm for corner-cutting tunneling calculations. *J. Chem. Phys.* **2001,** *114* (4), 1491-1496.
68. Fernández-Ramos, A.; Truhlar, D. G., A New Algorithm for Efficient Direct Dynamics Calculations of Large-Curvature Tunneling and Its Application to Radical Reactions with 9–15 Atoms. *J. Chem. Theory Comput.* **2005,** *1* (6), 1063-1078.
69. Martin, J. M. L., Ab initio total atomization energies of small molecules -- towards the basis set limit. *Chem. Phys. Lett.* **1996,** *259* (5-6), 669-678.
70. Feller, D.; Dixon, D. A., Extended benchmark studies of coupled cluster theory through triple excitations. *J. Chem. Phys.* **2001,** *115* (8), 3484-3496.
71. Morrison, R. T.; Boyd, R. N., *Organic Chemistry*. 6th ed.; Prentice-Hall, Inc.: New Jersey, 1992.

Table 1. Definition of the conformational reaction channels investigated in this study.

Name	Reactant	TS	Product	Reaction type
CRC01	PrOH_O	TS01	$CH_2O+CH_2CH_3$	C_α–C_β dissociation
CRC02	PrOH_C_α	TS02	$HOCHCH_2+CH_3$	C_β–C_γ dissociation
CRC03	PrOH_C_α	TS03	H + $OCHCH_2CH_3$	H–O dissociation
c-CRC04	PrOH_C_α	*c*-TS04	H + *cis*-$HOCHCHCH_3$	H–C_β dissociation
t-CRC04	PrOH_C_α	*t*-TS04	H + *trans*-$HOCHCHCH_3$	H–C_β dissociation
CRC05	PrOH_O	TS05	H + $OCHCH_2CH_3$	H–C_α dissociation
CRC06	PrOH_C_γ	TS06	CH_2OH + CH_2CH_2	C_α–C_β dissociation
CRC07	PrOH_O	TS07	PrOH_C_γ	H-migration
c-CRC08	PrOH_C_β	*c*-TS08	H + *cis*-$HOCHCHCH_3$	H–C_α dissociation
t-CRC08	PrOH_C_β	*t*-TS08	H + *trans*-$HOCHCHCH_3$	H–C_α dissociation
CRC09	PrOH_O	TS09	PrOH_C_α	H-migration
CRC10	PrOH_O	TS10	PrOH_C_β	H-migration
CRC11	PrOH_C_β	TS11	H + $HOCH_2CHCH_2$	H–C_γ dissociation
CRC12	PrOH_C_α	TS12	PrOH_C_β	H-migration
CRC13	PrOH_C_β	TS13	PrOH_C_γ	H-migration
CRC14	PrOH_C_α	TS14	PrOH_C_γ	H-migration
CRC15	PrOH_C_γ	TS15	H + $HOCH_2CHCH_2$	H–C_β dissociation
CRC16	PrOH_C_β	None	OH + CH_2CHCH_3	C_α–O dissociation

Table 2. Relative energies (including ZPE contributions) of the lowest-energy conformers of the reactants and transition states for the conformational reaction channels.

Name	Reactant	n_c	E (kcal mol^{-1})	TS	$n^{\ddagger}$	E (kcal mol^{-1})
CRC01	PrOH_O	2	5.9	TS01	2	25.9
CRC02	PrOH_C$_\alpha$	6	0.0	TS02	2	34.1
CRC03	PrOH_C$_\alpha$	6	0.0	TS03	3	36.6
c-CRC04	PrOH_C$_\alpha$	6	0.0	*c*-TS04	2	38.2
t-CRC04	PrOH_C$_\alpha$	6	0.0	*t*-TS04	2	38.4
CRC05	PrOH_O	2	5.9	TS05	3	32.5
CRC06	PrOH_C$_\gamma$	5	6.7	TS06	3	36.6
CRC07	PrOH_O	2	5.9	TS07	1	29.2
c-CRC08	PrOH_C$_\beta$	4	3.9	*c*-TS08	2	39.6
t-CRC08	PrOH_C$_\beta$	4	3.9	*t*-TS08	2	39.9
CRC09	PrOH_O	2	5.9	TS09	3	36.4
CRC10	PrOH_O	2	5.9	TS10	1	35.3
CRC11	PrOH_C$_\beta$	4	3.9	TS11	9	44.6
CRC12	PrOH_C$_\alpha$	6	0.0	TS12	4	43.4
CRC13	PrOH_C$_\beta$	4	3.9	TS13	9	44.1
CRC14	PrOH_C$_\alpha$	6	0.0	TS14	2	43.3
CRC15	PrOH_C$_\gamma$	5	6.7	TS15	9	45.9
CRC16	PrOH_C$_\beta$	4	3.9	None	-	-

Table 3. Rate constants (in s^{-1}) of the CRCs[a] and 1W/MP ratios calculated at 1500 K.

Channel	1W (eq 17)	1W (Zádor)[b]	MP (eq 12)	1W/MP	$n^{\ddagger}/n_C$
CRC01 (f)	9.34×10^{10}	4.37×10^{11}	8.43×10^{10}	1.11	2/2
CRC02 (f)	1.89×10^{9}	2.27×10^{9}	6.10×10^{8}	3.10	2/6
CRC03 (f)	3.60×10^{8}	2.34×10^{7}	1.93×10^{8}	1.87	3/6
c-CRC04 (f)	6.72×10^{7}	2.78×10^{8}	2.36×10^{7}	2.85	2/6
t-CRC04 (f)	8.01×10^{7}	2.46×10^{8}	2.45×10^{7}	3.27	2/6
CRC05 (f)	6.15×10^{9}	8.26×10^{10}	9.69×10^{9}	0.63	3/2
CRC06 (f)	2.17×10^{9}	1.10×10^{9}	1.11×10^{9}	1.95	3/5
CRC07 (f)	1.18×10^{9}	-	6.36×10^{8}	1.86	1/2
CRC07 (b)	4.69×10^{8}	1.66×10^{7}	7.43×10^{7}	6.32	1/5
c-CRC08 (f)	1.54×10^{8}	1.47×10^{8}	5.10×10^{7}	3.01	2/4
t-CRC08 (f)	8.26×10^{7}	1.40×10^{8}	3.27×10^{7}	2.52	2/4
CRC09 (f)	9.15×10^{8}	-	1.56×10^{9}	0.59	3/2
CRC09 (b)	5.83×10^{7}	3.32×10^{7}	2.93×10^{7}	1.99	3/6
CRC10 (f)	5.34×10^{8}	-	2.88×10^{8}	1.86	1/2
CRC10 (b)	4.52×10^{7}	-	8.35×10^{6}	5.41	1/4
CRC11 (f)	1.55×10^{7}	1.33×10^{5}	3.11×10^{7}	0.50	9/4
CRC12 (f)	1.17×10^{7}	-	7.14×10^{6}	1.64	4/6
CRC12 (b)	1.55×10^{7}	-	1.10×10^{7}	1.40	4/4
CRC13 (f)	9.18×10^{6}	-	1.65×10^{7}	0.56	9/4
CRC13 (b)	4.31×10^{7}	4.86×10^{7}	6.65×10^{7}	0.65	9/5
CRC14 (f)	5.43×10^{6}	-	1.46×10^{6}	3.72	2/6
CRC14 (b)	3.39×10^{7}	-	9.08×10^{6}	3.73	2/5
CRC15 (f)	2.74×10^{7}	2.02×10^{8}	4.17×10^{7}	0.66	9/5
CRC16 (f)[c]	3.52×10^{9}	1.68×10^{9}	6.50×10^{8}	5.41	-

[a] Letters "f" and "b" refer to forward and backward reactions, respectively. The last entry of the table is the ratio between the number of distinct TS conformers and that of reactant conformers (enantiomers are not included). [b] From Zádor and Miller.[43] [c] MP-CVT calculations.

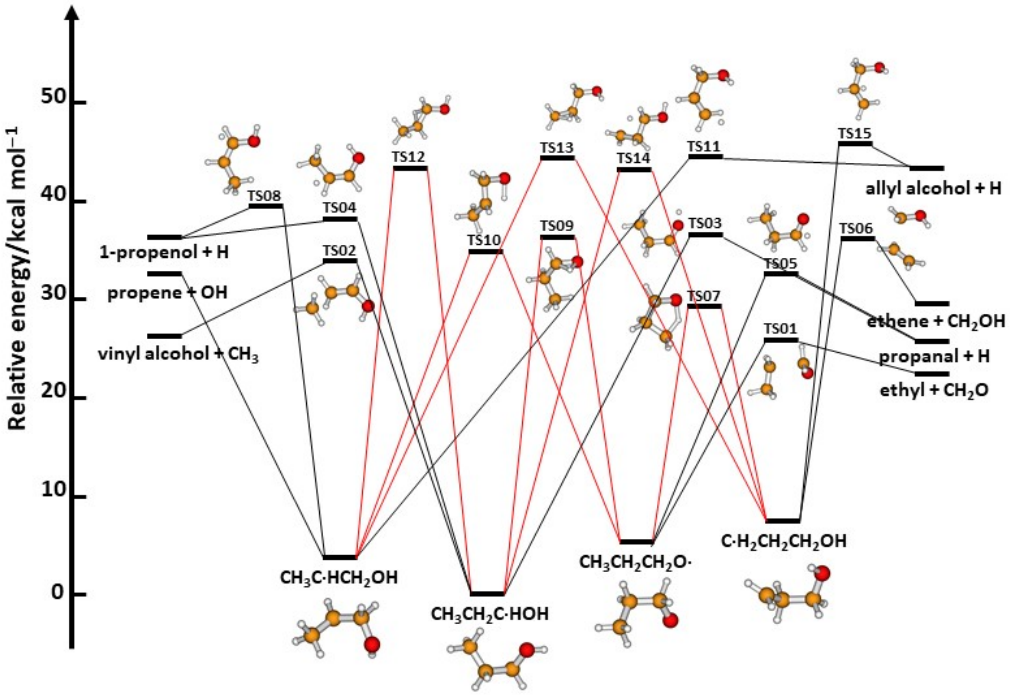

Figure 1. Simplified schematic diagram of the main reaction pathways in the dissociation of the 1-propanol radical. For clarity, the isomerization channels are depicted with red lines. Relative energies include ZPE contributions.

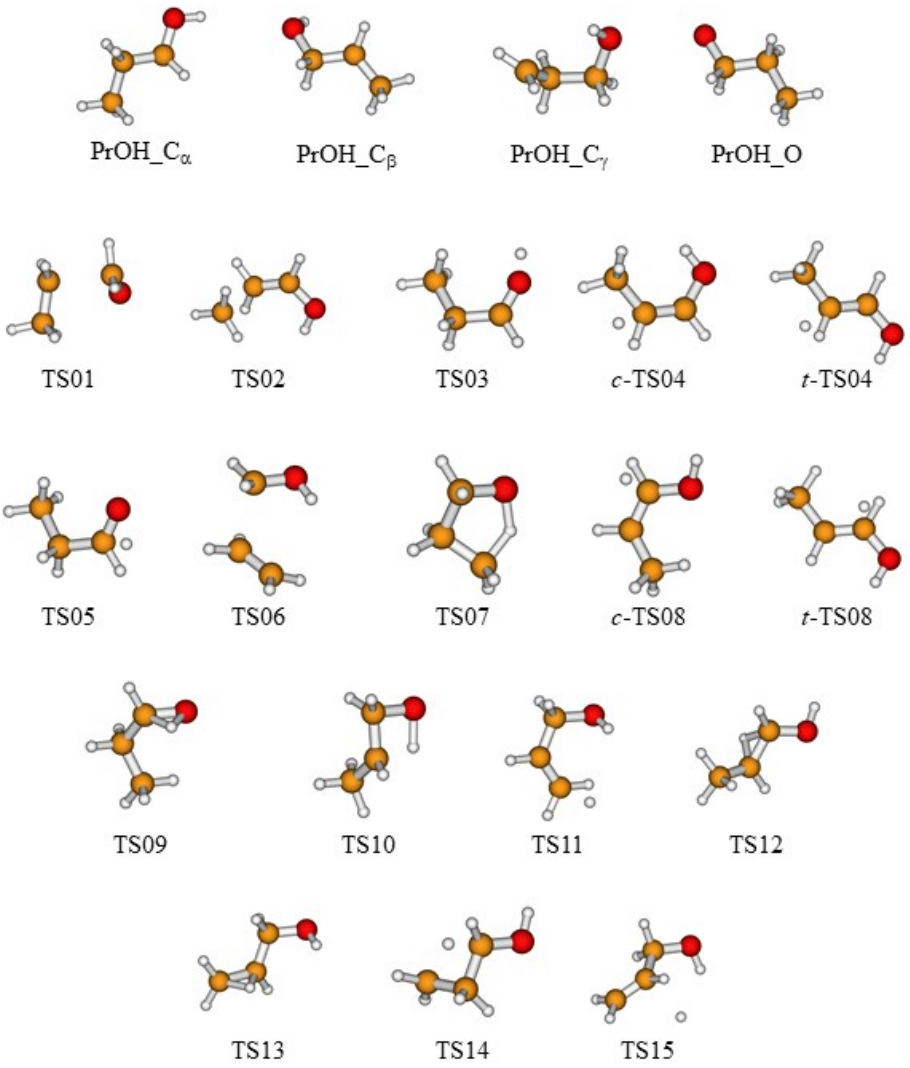

Figure 2. Drawings of the lowest-energy conformers of reactants and transition states for the conformational reaction channels investigated in this study.

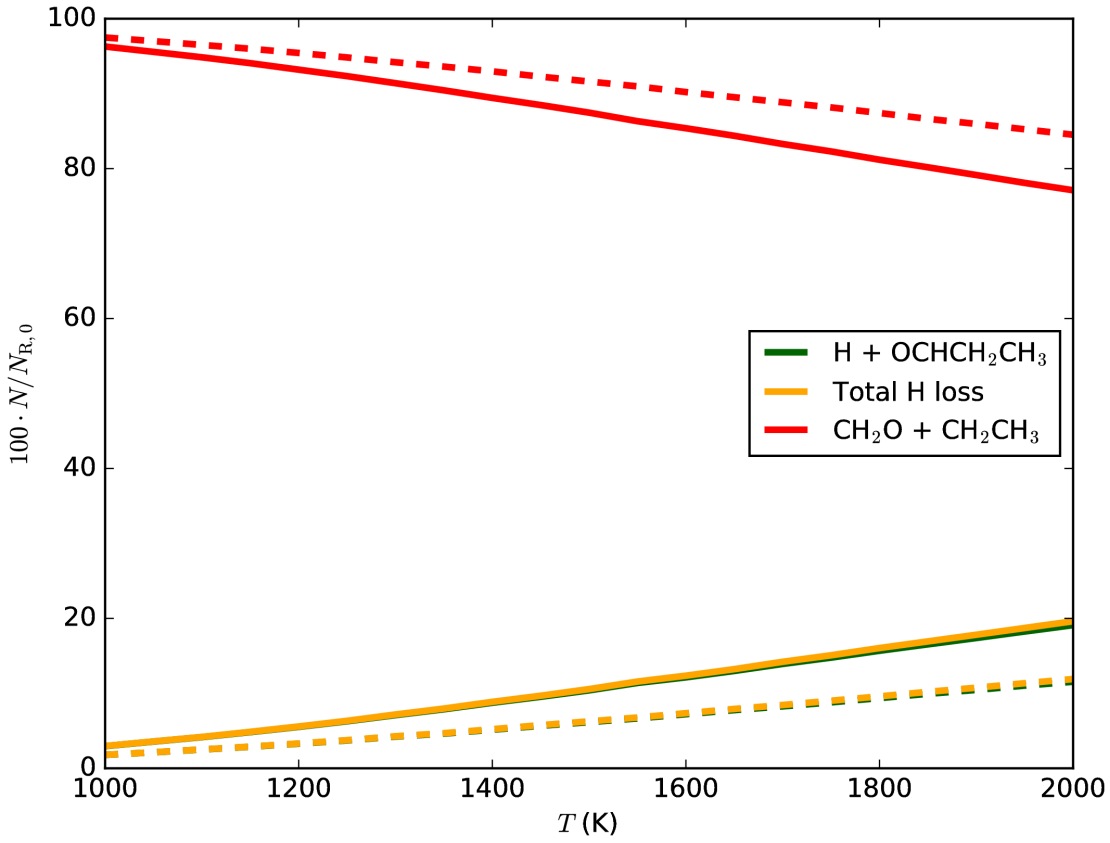

Figure 3. Product branching ratios obtained through KMC simulations starting from PrOH_O. Solid lines correspond to the MP simulations and dashed lines to those employing the 1W rate constants.

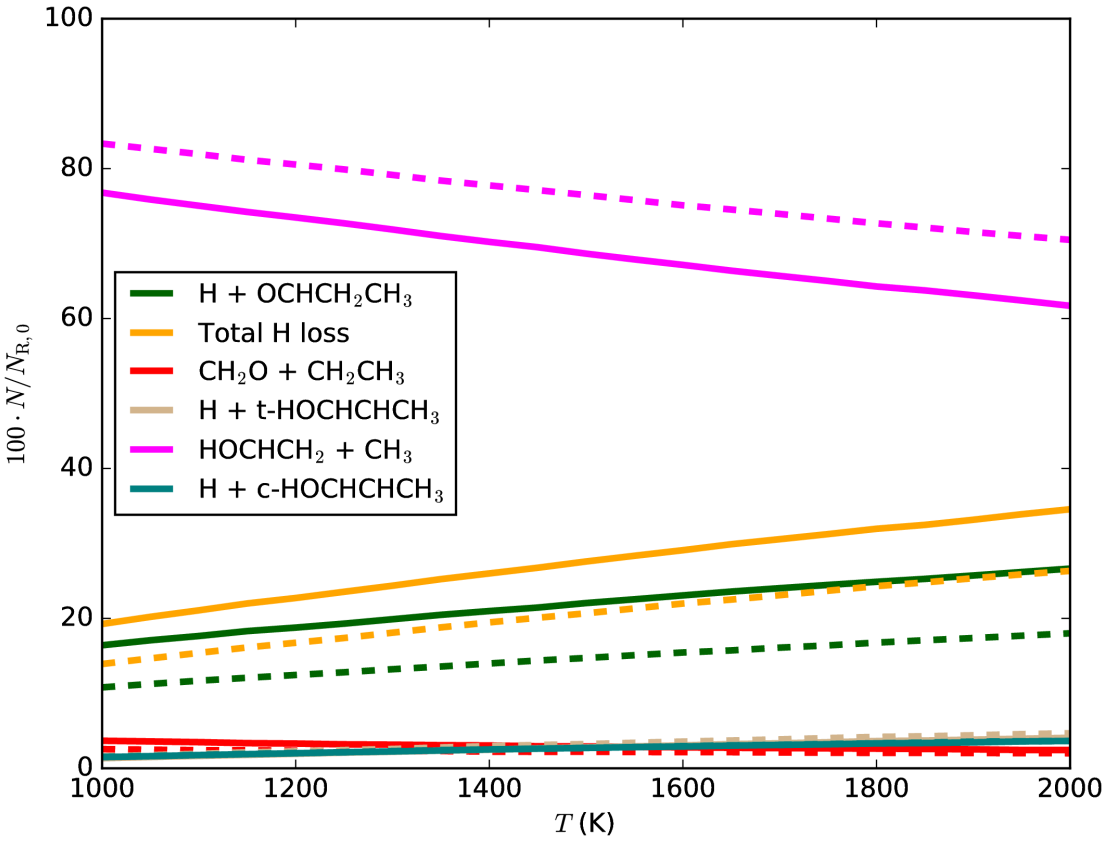

Figure 4. Product branching ratios obtained through KMC simulations starting from PrOH_C$_\alpha$. Solid lines correspond to the MP simulations and dashed lines to those employing the 1W rate constants.

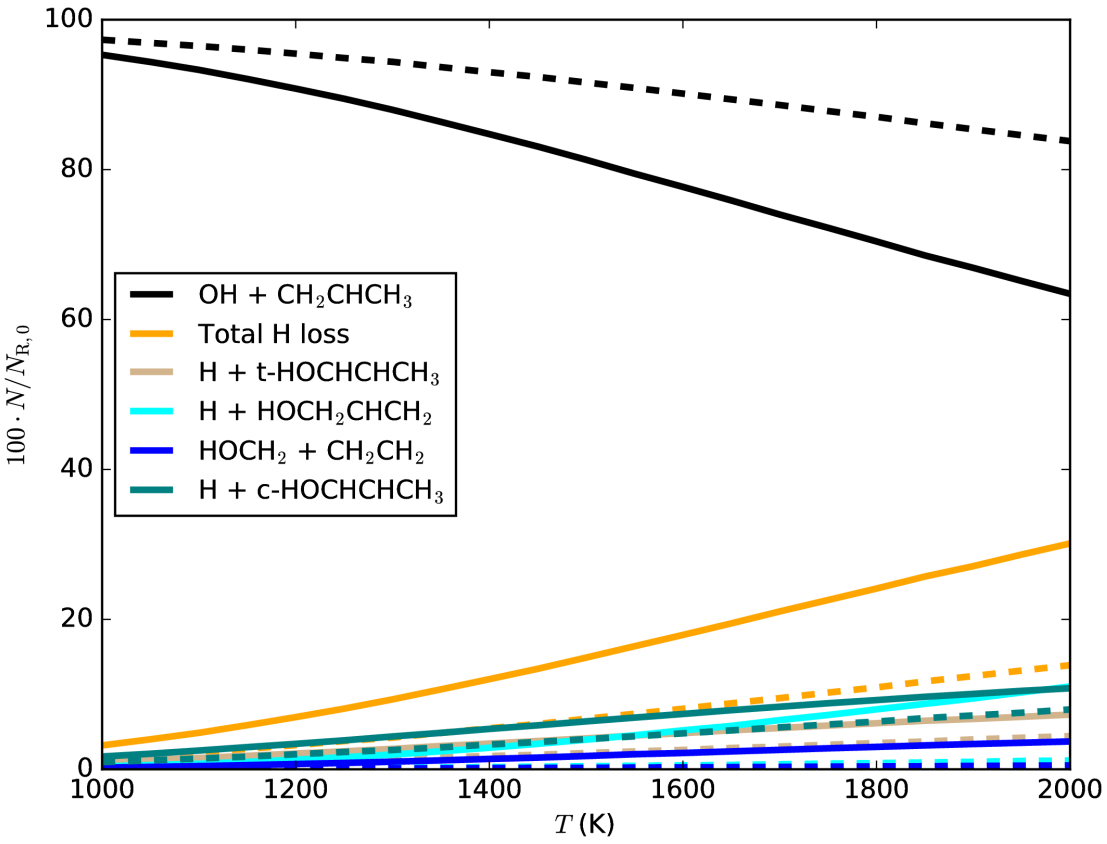

Figure 5. Product branching ratios obtained through KMC simulations starting from PrOH_C_β. Solid lines correspond to the MP simulations and dashed lines to those employing the 1W rate constants.

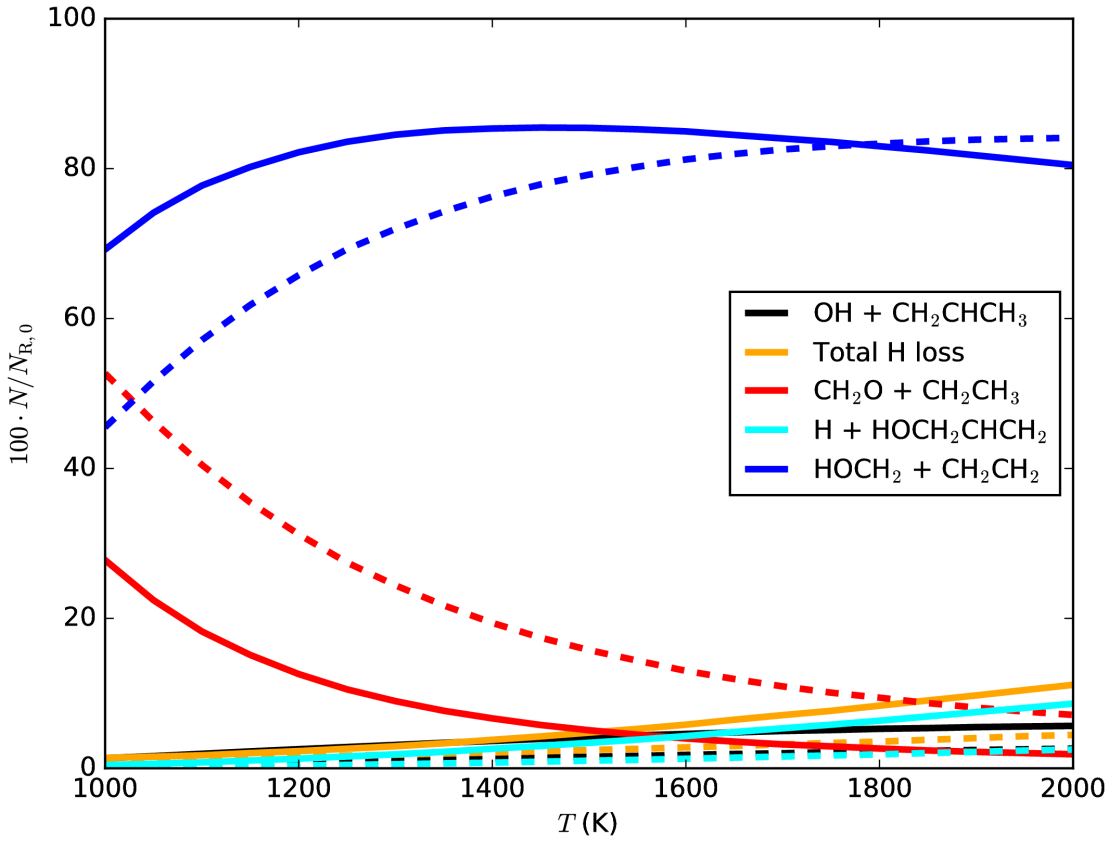

Figure 6. Product branching ratios obtained through KMC simulations starting from PrOH_C_γ. Solid lines correspond to the MP simulations and dashed lines to those employing the 1W rate constants.

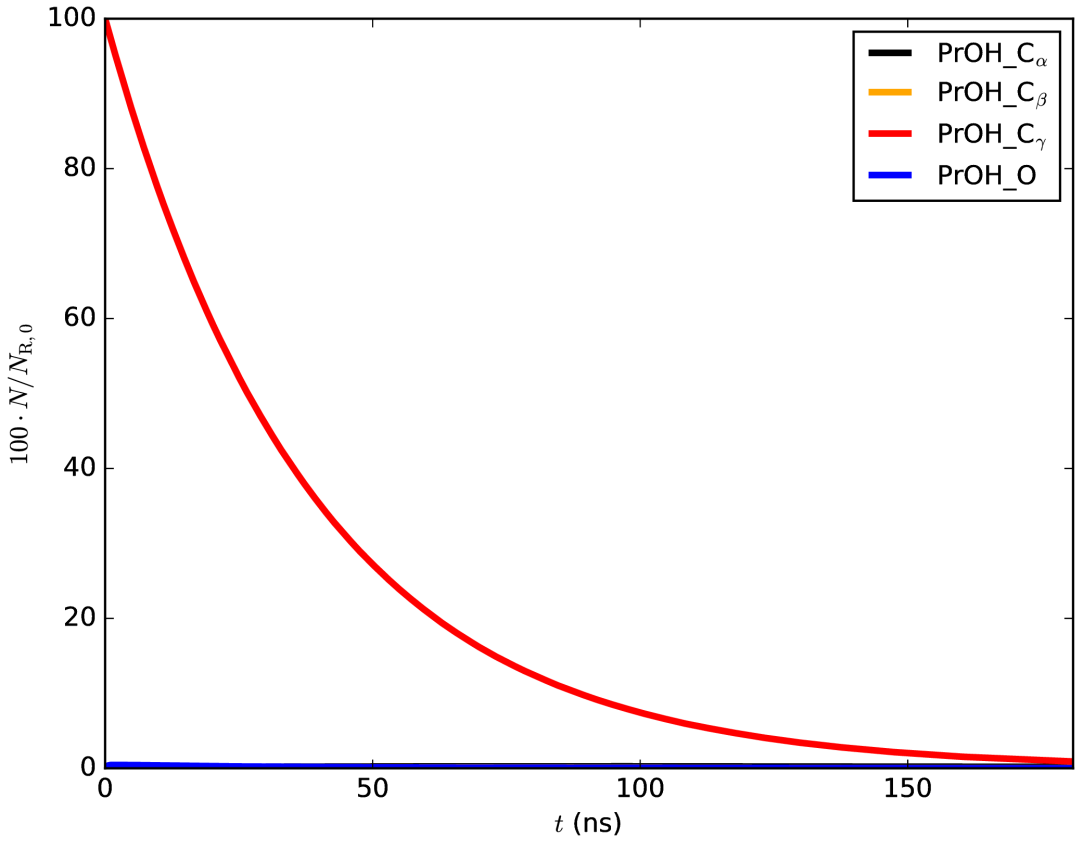

Figure 7. Ratios of the reactant radicals as a function of time obtained from a KMC simulation at 1000 K, using the 1W rate constants.

TOC graphic